Optical and structural properties of SiO x N y H z films deposited by electron cyclotron resonance and their correlation with composition

A. del Prado, E. San Andrés, I. Mártil, G. González-Diaz, D. Bravo, F. J. López, W. Bohne, J. Röhrich, B. Selle, and F. L. Martínez

Citation: Journal of Applied Physics **93**, 8930 (2003); doi: 10.1063/1.1566476
View online: http://dx.doi.org/10.1063/1.1566476
View Table of Contents: http://scitation.aip.org/content/aip/journal/jap/93/11?ver=pdfcov
Published by the AIP Publishing

Optical and structural properties of $SiO_xN_yH_z$ films deposited by electron cyclotron resonance and their correlation with composition

A. del Prado, E. San Andrés, I. Mártil, and G. González-Diaz
Departamento Física Aplicada III, Universidad Complutense de Madrid, 28040 Madrid, Spain

D. Bravo and F. J. López
Departamento Física de Materiales, Universidad Autónoma de Madrid, 28049 Madrid, Spain

W. Bohne, J. Röhrich, and B. Selle
Abt. Silizium-Photovoltaik und Ionenstrahl-Labor, Hahn-Meitner-Institut, 12489 Berlin, Germany

F. L. Martínez
Departamento Electrónica, Tecnología de Computadores y Proyectos, Universidad Politécnica de Cartagena, 30202 Cartagena, Spain

(Received 30 October 2002; accepted 19 February 2003)

$SiO_xN_yH_z$ films were deposited from O_2, N_2, and SiH_4 gas mixtures at room temperature using the electron cyclotron resonance plasma method. The absolute concentrations of all the species present in the films (Si, O, N, and H) were measured with high precision by heavy-ion elastic recoil detection analysis. The composition of the films was controlled over the whole composition range by adjusting the precursor gases flow ratio during deposition. The relative incorporation of O and N is determined by the ratio $Q=\phi(O_2)/\phi(SiH_4)$ and the relative content of Si is determined by $R=[\phi(O_2)+\phi(N_2)]/\phi(SiH_4)$ where $\phi(SiH_4)$, $\phi(O_2)$, and $\phi(N_2)$ are the SiH_4, O_2, and N_2 gas flows, respectively. The optical properties (infrared absorption and refractive index) and the density of paramagnetic defects were analyzed in dependence on the film composition. Single-phase homogeneous films were obtained at low SiH_4 partial pressure during deposition; while those samples deposited at high SiH_4 partial pressure show evidence of separation of two phases. The refractive index was controlled over the whole range between silicon nitride and silicon oxide, with values slightly lower than in stoichiometric films due to the incorporation of H, which results in a lower density of the films. The most important paramagnetic defects detected in the films were the K center and the E' center. Defects related to N were also detected in some samples. The total density of defects in $SiO_xN_yH_z$ films was higher than in SiO_2 and lower than in silicon nitride films.
 [DOI: 10.1063/1.1566476]

I. INTRODUCTION

Silicon oxynitride is a very interesting material for the microelectronics industry due to the possibility to obtain intermediate properties between silicon oxide and silicon nitride.

Silicon oxide is widely used as gate dielectric in metal–insulator–semiconductor devices and thin film transistors. However, the decrease of the oxide thickness as the scale of integration increases, results in too high tunnel currents and the diffusion of Boron or p-type dopants from the gate.[1,2] The incorporation of N to the oxide increases the dielectric permittivity, so that physically thicker films can be deposited, with the same equivalent oxide thickness, reducing the tunnel currents. Furthermore, the barrier properties against diffusion are improved, as well as the reliability of the devices.[1,3,4]

Additionally, by an adequate control of the composition of silicon oxynitride, it is possible to obtain a lower mechanical stress than in silicon nitride, which is of great interest for its application as passivation dielectric in multilevel metallization processes.[5]

Finally, the possibility to control the refractive index between the silicon nitride and silicon oxide values allows several optical applications, such as graded index films or antireflection coatings.[6–8]

Concerning the growth of silicon oxynitride films (in the following $SiO_xN_yH_z$), research is mainly focused on those techniques with a low thermal budget, according to the requirements of ultralarge scale integration technology, such as rapid thermal processing[4,9,10] or different Plasma Enhanced Deposition techniques.[1,5,6,11–15] Among these, the electron cyclotron resonance plasma chemical vapor deposition (ECR-PECVD) method shows several interesting advantages in addition to the low temperature requirement. It does not require the presence of a cathode, which is specially important in processes using corrosive gases. Substrates are placed outside the plasma region, so that damage due to ion bombardment is reduced. Finally, a very high activation of the precursor gases is achieved, which allows the use of N_2 instead of NH_3 as a source of N atoms, thus reducing the incorporation of H to the films.

In this work the properties of $SiO_xN_yH_z$ thin films deposited by ECR-PECVD at room temperature are studied. By

TABLE I. Precursor gas flow ratios for the different samples. $R=[\phi(O_2)+\phi(N_2)]/\phi(SiH_4)$ and $Q=\phi(O_2)/\phi(SiH_4)$. Total gas flow was set at 10.5 sccm.

Sample series	R	Q
R0.88	0.88	0.13–0.79
R1.6	1.6	0–1.6
R5.0	5.0	0–5.0
R9.1	9.1	0–4.5
Q0.8	0.88–10.7	0.8

using a wide range of different gas flow ratios during deposition, samples of very different compositions and properties were obtained. The combination of accurate composition measurements by heavy-ion elastic recoil detection analysis (HI-ERDA), with techniques for optical and structural characterization, such as Fourier transform infrared (FTIR) spectroscopy, ellipsometry, and electron paramagnetic resonance (EPR), has allowed a detailed study of the correlation between deposition parameters, film composition, and the optical and structural properties.

II. EXPERIMENT

The films were deposited using a commercial ECR reactor (Astex AX4500) attached to a stainless steel deposition chamber. O_2, N_2 (which are fed directly into the plasma chamber) and SiH_4 (which is introduced into the deposition chamber by means of a dispersal ring) were used as precursor gases. The flow was controlled by mass flow controllers. More details on the deposition system are given elsewhere.[16]

In all depositions the total gas flow, pressure and microwave power were kept constant at 10.5 sccm, 9×10^{-4} mbar, and 100 W, respectively. The substrates were not intentionally heated and the deposition temperature was about 50 °C.

Samples of different compositions were obtained by changing the flow ratio of the precursor gases. To characterize the deposition process the parameters $R=[\phi(O_2)+\phi(N_2)]/\phi()SiH_4)$ and $Q=\phi(O_2)/\phi(SiH_4)$ were used, where $\phi(SiH_4),\phi(O_2)$, and $\phi(N_2)$ are the SiH_4, O_2, and N_2 gas flows, respectively. As the total flow is constant, the parameter R determines the SiH_4 partial pressure during deposition, with the highest SiH_4 pressure for the lowest value of R. The parameter Q controls the relative flow of O_2 and N_2 for a given value of R. Table I summarizes the gas flows used for the different sample series deposited in this work. Along the article, samples will be named according to the values of the parameters R and Q used during deposition (for instance, sample R1.6Q0.80 means that it has been deposited at $R=1.6$ and $Q=0.80$).

The samples were deposited on high resistivity (80 Ω cm) *p*-type Si(111) substrates. The substrates were cleaned using standard procedures.[17] The thickness of the films was about 300 nm.

The composition of the samples of series R1.6 and R5.0 (see Table I) was measured with the HI-ERDA technique, using 150 MeV $^{86}Kr^{+}$ ions. The identification of the species present in the film was performed using the time of flight technique. This technique allows the determination of the absolute concentrations of all the species present in the $SiO_xN_yH_z$ films, including H, without need of any reference sample, with a very high sensitivity (0.01 at. %) and precision (about 3%). Details on the HI-ERDA setup and the measurements are given elsewhere.[18,19]

The bonding structure of the films was investigated by FTIR spectroscopy. A Nicolet 5PC spectrometer operating at normal incidence and transmission mode was used for the measurements. Additionally, the bonded H content was evaluated from the Si–H and N–H stretching bands using the calibration factors calculated by Lanford and Rand.[20]

The thickness of the films and the refractive index at the He–Ne laser wavelength (632.8 nm) were measured by ellipsometry, using a Plasmos E2302 ellipsometer with incidence and detection angles both set at 70°.

Finally, the density of paramagnetic defects was determined by EPR measurements, using a Bruker ESP 300E *X* band spectrometer. The microwave power was set at 0.5 mW to avoid saturation of the signal and the density of defects was evaluated using a weak pitch standard. For these measurements stacks of films deposited in the same process for a total thickness between 1500 and 2500 nm were used.

III. RESULTS

A. Composition (HI-ERDA) measurements

As the main interest of $SiO_xN_yH_z$ is the control of its properties between those of silicon nitride and oxide, it appeared to be useful to deal with a parameter which could serve as an indicator of how close the composition is to either silicon nitride or silicon oxide.

For stoichiometric silicon oxynitride films, SiO_xN_y, with no H content and only Si–O and Si–N bonds present in the films, such a parameter (which we will call α) can be defined as the ratio between the concentration of Si–O bonds and the total concentration of bonds:

$$\alpha=\frac{[\mathrm{Si{-}O}]}{[\mathrm{Si{-}O}]+[\mathrm{Si{-}N}]}=\frac{2[\mathrm{O}]}{2[\mathrm{O}]+3[\mathrm{N}]}=\frac{2x}{2x+3y} \qquad (1)$$

where the coordination numbers of O and N have been taken into account.

This parameter α can be understood as the fraction of oxide present in the SiO_xN_y film, so that $\alpha=0$ corresponds to $SiN_{1.33}$, $\alpha=1$ to SiO_2, and $\alpha=0.5$ is the exact middle composition. The meaning of α may be better understood if the SiO_xN_y formula is written as $(SiO_2)_\alpha(SiN_{1.33})_{1-\alpha}$. Note that writing the silicon oxynitride formula in this way does not imply a separation of two phases in the films. This subject will be discussed in the following section. Furthermore, this parameter α correlates with the relative concentration of the SiO_jN_{4-j} tetrahedron units in the random bonding model (RBM).[21]

For samples containing H, which deviate from the stoichiometric composition, the parameter α given by Eq. (1) is not exactly the oxide fraction as explained above, and a correction should be made. For instance, for samples with a concentration of N–H bonds proportional to the N content, i.e., $[\mathrm{N{-}H}]=X_{\mathrm{NH}}[\mathrm{N}]$, but no significant concentrations of Si–Si or Si–H bonds, the oxide fraction would be given by[22]

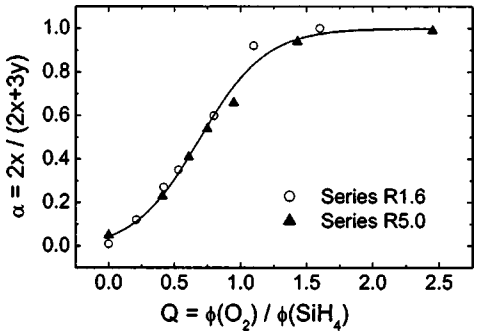

FIG. 1. Composition parameter α [Eq. (1)] as a function of the deposition gas flow ratio $Q=\phi(O_2)/\phi(SiH_4)$ for series R1.6 and R5.0, deposited at different SiH_4 partial pressures. Line is drawn as a guide to the eye.

$$\alpha' = \frac{[\text{Si–O}]}{[\text{Si–O}]+[\text{Si–N}]} = \frac{2x}{2x+(3-X_{\text{NH}})y}. \tag{2}$$

For low H content, the differences between the parameter α [Eq. (1)] and the corrected value α' [Eq. (2)] are almost negligible (below 3% for our samples). So, to simplify matters, the value of the parameter α given by Eq. (1) is used in the following to characterize the composition of our films.

The control of the composition is realized by adjusting the gas flow ratios during deposition. Figure 1 shows the measured composition parameter α as a function of the gas flow ratio $Q=\phi(O_2)/\phi(SiH_4)$, for samples of series R1.6 and R5.0, deposited at different SiH_4 partial pressures. As shown in the figure, the oxide fraction α is mainly determined by the parameter Q, regardless of the value of R.

The measured concentrations (at. %) of each of the species present in the $SiO_xN_yH_z$ films (Si, O, N, and H) are shown in Fig. 2 as a function of the composition parameter α, for samples of series R1.6 and R5.0. The expected concentrations for stoichiometric SiO_xN_y (with no H content and only Si–O and Si–N bonds, so that the relation $2x+3y=4$ is verified)[11] are also shown as solid lines for comparison. While the obtained O content is essentially the same as in stoichiometric films, both the Si and N contents are slightly lower, especially for compositions close to silicon nitride. This result is related to the presence of H, which is higher for those compositions.

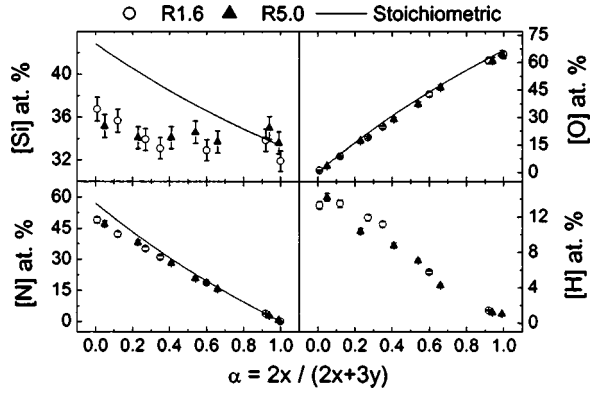

FIG. 2. Atomic percentages of Si, O, N, and H, measured by HI-ERDA, for series R1.6 and R5.0 as a function of the composition parameter α [Eq. (1)]. The calculated values for stoichiometric SiO_xN_y films are shown as solid lines.

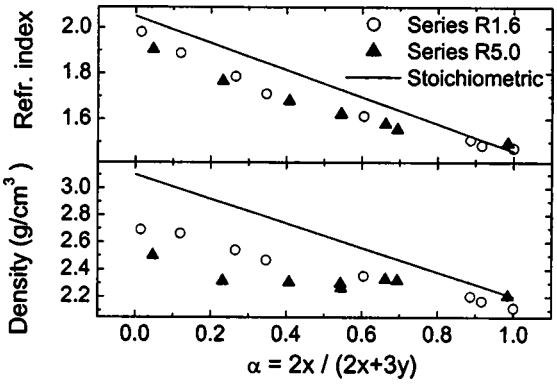

FIG. 3. Refractive index (upper) and mass density of the films (lower) as a function of the composition parameter α for samples of series R1.6 and R5.0. The solid lines correspond to the calculated values for stoichiometric SiO_xN_y films.

B. Ellipsometry measurements

Figure 3 shows the mass density (ρ) of the films, calculated from the HI-ERDA results and the thickness obtained by ellipsometry, as a function of composition, for samples of series R1.6 and R5.0. The refractive index (n), measured at $\lambda=632.8$ nm is also shown in Fig. 3. The density and refractive index values corresponding to stoichiometric H-free SiO_xN_y are plotted as solid lines for comparison. These curves were calculated taking $\rho=2.2$ g cm^{-3} and $n=1.46$ for SiO_2,[23] and $\rho=3.1$ g cm^{-3} and $n=2.05$ for Si_3N_4,[23] and assuming a linear dependence on the parameter α.

Both the density and the refractive index of the deposited samples are slightly lower than the expected for stoichiometric films. According to the work of Sassella *et al.*[24] the refractive index in $SiO_xN_yH_z$ films is related to the mass density, so that a decrease in the density results in a decrease of the refractive index. As shown in Fig. 2, the incorporation of H results in lower concentrations of Si and N in our samples than in stoichiometric ones, which in turn results in a lower density. We attribute the lower refractive index values to this lower density of the films.

Deposition rate was also calculated from the measured thickness. The deposition rate is mainly determined by the parameter $R=[\phi(O_2)+\phi(N_2)]/\phi(SiH_4)$, which controls the SiH_4 partial pressure. Figure 4 shows the deposition rate for samples of series Q0.8 as a function of R. For R values up to $R=1.5$, high deposition rates (above 15 nm/min) are observed. For greater values of $R(R>3)$ the deposition rate significantly drops down.

C. FTIR spectroscopy measurements

1. Si–H and N–H stretching bands

The Si–H and N–H bond concentrations for samples of series Q0.8 are shown in Fig. 4, as a function of the parameter R, together with the deposition rate. The bond concentrations were evaluated from the Si–H and N–H stretching

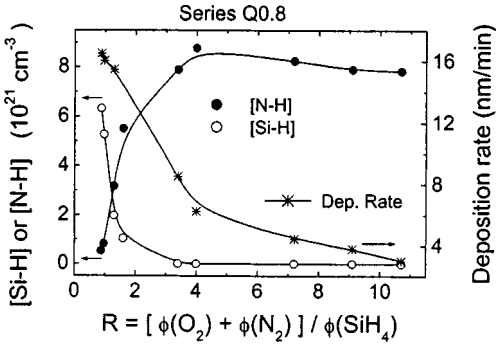

FIG. 4. Si–H and N–H bond concentrations and deposition rate as a function of the gas flow ratio $R=[\phi(O_2)+\phi(N_2)]/\phi(SiH_4)$ for series Q0.8. Lines are drawn as a guide to the eye.

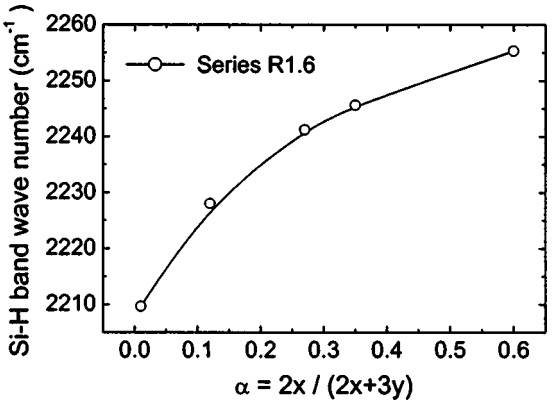

FIG. 6. Wave number of the Si–H stretching band as a function of the composition parameter α, for samples of series R1.6. Line is drawn as a guide to the eye.

absorption bands, using the calibration factors given by Lanford and Rand.[20] For R values below 1, the Si–H concentration is much higher than the N–H concentration, suggesting that these samples may be Si rich. On the other hand, for greater values of R, the N–H concentration is higher, with a negligible Si–H concentration for $R>3$.

By the term ''Si rich'' we understand samples with a relative content of Si higher than in stoichiometric films, with respect to N and O (i.e., $2x+3y<4$). Still, the presence of H may result in a lower total Si content than in stoichiometric films, in a similar way as shown in Fig. 2.

In addition to the H concentration obtained from the area of the absorption bands, the FTIR spectroscopy measurements provide useful information about the structure of bonds of the films. In particular, the Si–H stretching band is very sensitive to the chemical environment of the Si–H bond, so that as the electronegativity of the neighbor atoms increases, the band shifts to higher wave numbers.[25–27]

Figure 5 shows the absorption spectrum in the Si–H stretching band range for several samples. The composition for the sample deposited at $R=0.88$ and $Q=0.49$ is very close to silicon nitride. A single band located about $\nu_{SiH}=2168$ cm^{-1} is observed. This value is intermediate between the value for the $(SiN_2)-Si-H$ configuration ($\nu_{SiH}=2140$ cm^{-1})[25,27] and the $(N_3)-Si-H$ configuration ($\nu_{SiH}=2200$ cm^{-1}),[25,27] which supports the conclusion that for this low value of R Si-rich films (or films with an excess Si content with respect to stoichiometric samples) are obtained.

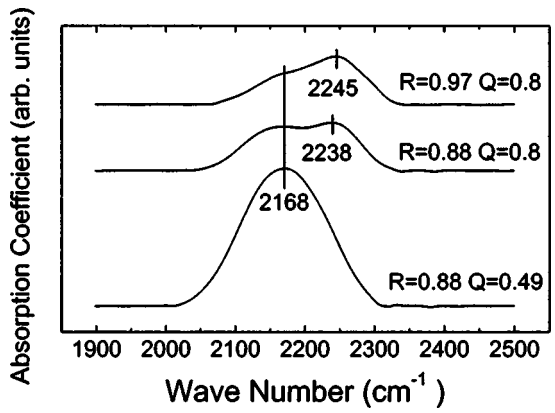

FIG. 5. Absorption spectrum (Si–H stretching band) for three representative samples deposited at $R<1$.

For $R=0.88$ and $Q=0.8$, an intermediate composition between nitride and oxide is obtained. For this sample two peaks can be resolved, one located at $\nu_{SiH}=2168$ cm^{-1}, characteristic of Si-rich silicon nitride, as explained above, and the other located at $\nu_{SiH}=2238$ cm^{-1}, which is slightly lower than the frequency corresponding to the $(O_3)-Si-H$ configuration ($\nu_{SiH}=2245-2265$ cm^{-1})[25–28] in SiO_2. The lower value observed in our work is attributed to contributions of configurations in which O atoms are substituted by Si atoms, such as $(SiO_2)-Si-H$ ($\nu_{SiH}=2180-2195$ cm^{-1}).[25–28]

The behavior of the sample deposited at $R=0.97$ and $Q=0.8$ is very similar to the previous one, although for this sample the oxide peak slightly shifts to higher wave numbers, due to the lower Si content in this sample, and the nitride peak becomes less clear, probably also due to the lower Si concentration, so that the contribution of $(SiN_2)-Si-H$ groups is less significant and the wave number of the band approaches 2200 cm^{-1}.

For samples deposited at higher values of R, the Si–H band shows essentially a single peak that shifts to higher wave numbers as the composition changes from silicon nitride to silicon oxide, due to the higher electronegativity of O with respect to N.[25] This behavior is shown in Fig. 6 for the samples of series R1.6.

2. Si–O/Si–N stretching band

We have studied the absorption spectrum of our deposited $SiO_xN_yH_z$ films as a function of the deposition parameters. Figure 7 shows the IR spectra in the 400–1400 cm^{-1} range for samples deposited at $Q=0.8$ (series Q0.8), for which intermediate compositions are obtained, as a function of R.

For the lowest values of R ($R<1$) two peaks are clearly distinguished, one located at 872 cm^{-1}, close to the characteristic value for the Si–N stretching vibration in Si_3N_4 (835 cm^{-1}), and the other at 1026 cm^{-1}, close to the value for the Si–O stretching vibration in SiO_2 (1075 cm^{-1}).

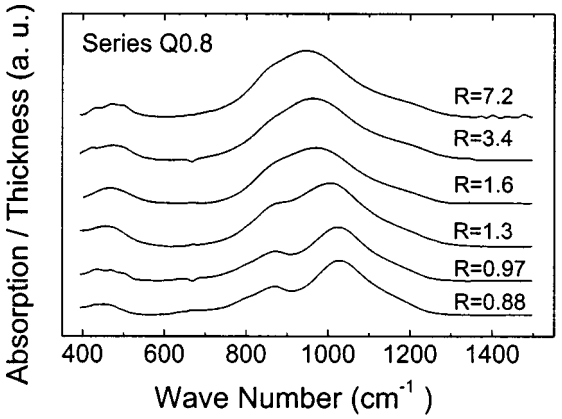

FIG. 7. Absorption spectrum (Si–O/Si–N stretching band) for series Q0.8 for different values of R.

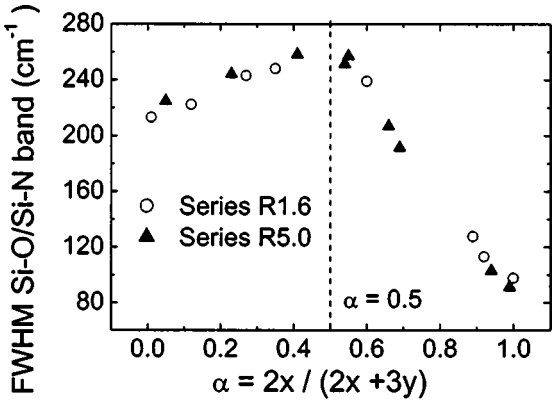

FIG. 9. FWHM of the Si–O/Si–N stretching band as a function of the composition parameter α for samples of series R1.6 and R5.0.

For higher values of R, the separation of the two peaks becomes gradually less pronounced, with a single peak being observed for $R>3$.

Figure 8 shows the absorption spectra for samples of series R5.0, (deposited at $R=5.0$), for different values of the parameter Q. As Q is increased (the composition changes from silicon nitride to oxide) the band continuously shifts from the characteristic nitride value to the oxide value.

For the samples showing a single Si–O/Si–N stretching band, another important parameter is the full width at half maximum (FWHM) of this band. This parameter is related to the structural order of the film and the dispersion of different chemical environments, with higher values of the FWHM indicating higher disorder and higher dispersion of different environments.[29,30]

Figure 9 shows the FWHM of the Si–O/Si–N stretching band for samples of series R1.6 and R5.0 as a function of the composition parameter α. As composition changes from silicon nitride to silicon oxide, the FWHM increases until reaching a maximum value for intermediate compositions, and then decreases. The same behavior has been reported by other authors.[11,30] The maximum value of the FWHM is obtained for values of α around 0.5, suggesting that the maximum dispersion of different chemical environments corresponds to this composition.

One of the most extended models to describe the bonding structure of the $SiO_xN_yH_z$ is the random bonding model (RBM) originally proposed by Philipp.[31] According to this model, the silicon oxynitride is formed by tetrahedral structural units, with a Si atom at the center and different occupation of the vertices of the tetrahedron by N and O atoms. The five fundamental tetrahedrons may be indexed according to the number of N or O atoms present: SiO_jN_{4-j}, with $j=0, 1, 2, 3, 4$. Neglecting the presence of H, the probability P_j or relative concentration of each tetrahedron is given by[21]

$$P_j=\binom{4}{j}\alpha^j(1-\alpha)^{4-j}. \tag{3}$$

The dielectric function of the SiO_xN_y and, therefore, the absorption coefficient can be obtained by combining the dielectric function of each fundamental tetrahedron according to the effective medium theory.[21] In addition, the presence of bonded H or Si–Si bonds can be taken into account by increasing the possible types of tetrahedrons, so that Si–H, N–H and Si–Si bonds are included.[24,32]

In order to study the dispersion of different chemical environments, the probability P_j calculated from equation (3) for α values in the range from 0 to 0.5 is shown in Fig. 10. (Note that for $\alpha>0.5$, the distribution of tetrahedrons would be equivalent to that for $1-\alpha$, exchanging $j=0$ for $j=4$ and $j=1$ for $j=3$). Although the shape of the Si–O/Si–N absorption band is not only determined by the relative

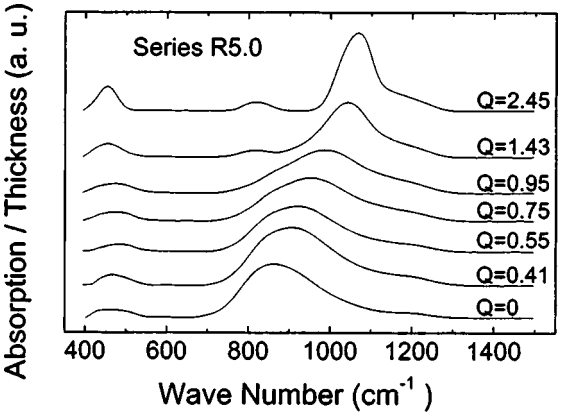

FIG. 8. Absorption spectrum (Si–O/Si–N stretching band) for series R5.0 for different values of Q.

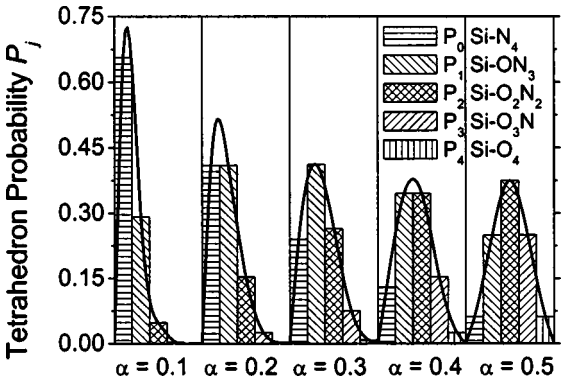

FIG. 10. Probability P_j of each tetrahedron of the type SiO_jN_{4-j}, according to the RBM [Eq. (3)], for different values of the composition parameter α. Lines are drawn as a guide to the eye.

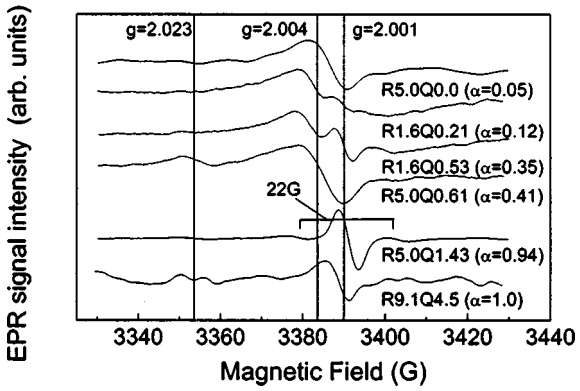

FIG. 11. EPR spectra of selected $SiO_xN_yH_z$ samples with different composition.

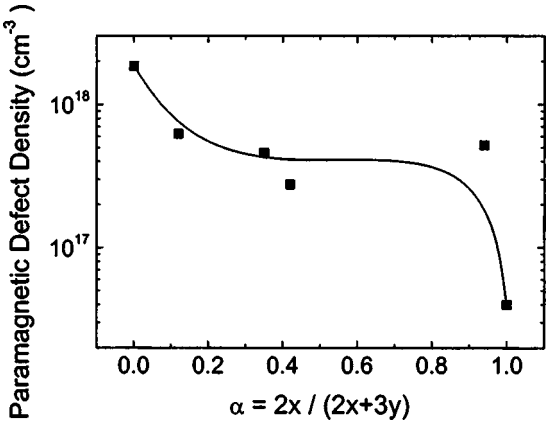

FIG. 12. Overall paramagnetic defect density as a function of the composition parameter α. Line is drawn as a guide to the eye.

concentrations of the different tetrahedrons, but also by the oscillator strength and resonance width of the dielectric function of each tetrahedron,[21] it is clear in Fig. 10 that the maximum dispersion of different tetrahedrons is obtained for values of α around 0.5. The validity of the RBM for our films will be discussed later.

D. EPR measurements

The density of defects with paramagnetic activity in the films was studied by EPR. Figure 11 shows representative EPR spectra for samples deposited at different gas flow ratios. The derivative spectrum is shown, and the resonance condition for the absorption is[33]

$$h\nu = g\mu_B B, \tag{4}$$

where ν is the microwave frequency (ν=9.5 GHz), μ_B is the Bohr magnetron, B is the applied magnetic field, and g is the spectroscopic splitting factor, characteristic of each defect.

The composition of sample R5.0Q0.0 is essentially silicon nitride (α=0.05). The EPR spectrum of this sample shows a dominant feature with a g factor around $g=2.004$. This signal is attributed to the K center ($N_3{\equiv}Si\uparrow$, $g=2.0028$) with possible contributions in which N atoms are substituted by Si atoms, such as $SiN_2{\equiv}Si\uparrow$, $Si_2N{\equiv}Si\uparrow$, or even $Si_3{\equiv}Si\uparrow$. For these configurations the value of g increases from 2.0028 for $N_3{\equiv}Si\uparrow$ to 2.0055 for $Si_3{\equiv}Si\uparrow$.[34]

For silicon oxide, (sample R9.1Q4.5, α=1.0), the characteristic signal of the E' center ($O_3{\equiv}Si\uparrow$, $g=2.0018$) is observed.[35]

For samples of intermediate composition, the behavior is different depending on the value of the gas flow ratio R. For those samples deposited at $R=1.6$, two signals can be distinguished in the EPR spectrum; one close to the characteristic g value of the K center and the other corresponding to the E' center. On the other hand, for sample R5.0Q0.61 (α =0.41), deposited at a high R value, the EPR signal does not split up and shows a single feature located at $g=2.004$. This signal is due to the Si dangling bond. The high observed value of g suggests that the signal is mainly due to defects similar to the K center, rather than defects with a configuration similar to that of the E' center. A weak signal is also observed around $g=2.023$. This signal is very close to one of the three characteristic lines of the N dangling bond defect. The most intense signal of this defect is located at $g=2.0055$ and the third very weak line appears at lower values of g.[36] Therefore, the line observed at $g=2.023$ in the spectrum of Fig. 11 for sample R5.0Q0.61 (α=0.41) is tentatively attributed to the N dangling bond center, with the principal line of the defect masked in the dominant signal around $g=2.004$. The third line may be too weak to be distinguished from noise.

Finally, the EPR spectrum of sample R5.0Q1.43, of composition very close to silicon oxide (α=0.94) shows some interesting features. The intense signal appearing at $g=2.0008$ is attributed to an E'-like center where an O atom is substituted by a Si atom ($SiO_2{\equiv}Si\uparrow$).[37] Additionally, a weak doublet with a separation of 22 G is observed. Similar structures have been observed by other authors in silicon oxide films and attributed to defects related to N.[38,39] In fact, these defects show a spectrum with three lines, but in our samples the central line is masked by the intense signal at $g=2.0008$. Since we have not detected this doublet in N-free SiO_x samples,[40] we conclude that this 22 G doublet is related to the presence of N in the film. The defect may be in fact the N_4^0 center, as explained by Stathis *et al.*[38]

Figure 12 shows the total concentration of paramagnetic defects as a function of composition. The highest defect density is obtained for silicon nitride films (α=0). For $SiO_xN_yH_z$ films the defect density is lower than in nitride films and remains roughly constant over the whole composition range. For SiO_2 samples (α=1) the density of defects significantly decreases with respect to $SiO_xN_yH_z$ films. While the incorporation of O to SiN_yH_z films seems to have a beneficial effect, the incorporation of N to the SiO_2 results in a significant increase of the density of defects. It must be noted, however, that defects with no paramagnetic activity may also be present in the films.

IV. DISCUSSION

A. Control of composition

According to the results shown in Figs. 1 and 2, it becomes apparent that our ECR-PECVD process is capable of producing films with well controlled compositions over the whole range between silicon nitride (α=0) and silicon oxide (α=1). It must also be noted that it has been possible to

obtain compositions close to SiN_yH_z with relatively low $\phi(N_2)/\phi(O_2)$ ratios (for instance, for the sample deposited at $R=1.6$ and $Q=0.21$, the value $\alpha=0.12$ is obtained with $\phi(N_2)/\phi(O_2)=6.7$). Keeping the flows of all the precursor gases in the same order of magnitude makes the control more reliable, enhancing the reproducibility of the deposition process. This is possible due to the high activation efficiency of the ECR plasma, which allows an efficient activation of N_2.

The control of the composition allows to control the refractive index between the silicon nitride value ($n=1.98$ for our samples) and the silicon oxide value ($n=1.46$), as shown in Fig. 3. This is of special interest for optical applications, such as graded index films or antireflection coatings.[6–8]

The composition parameter α is mainly determined by the O_2 to SiH_4 gas flow ratio $Q=\phi(O_2)/\phi(SiH_4)$, regardless of the value of the parameter $R=[\phi(O_2)+\phi(N_2)]/\phi(SiH_4)$, as evidenced by Fig. 1.

However, the parameter R has also a very important influence on the properties of the deposited films. For SiN_yH_z samples, deposited in the same reactor and under the same conditions, R determines the relative N and Si content.[41] For low values of R (high SiH_4 partial pressure) Si-rich films are obtained, while for high values of R (low SiH_4 partial pressure) N-rich films are obtained. Additionally, for Si-rich films, the Si–H bond concentration is higher than the N–H bond concentration, while the opposite result ([N–H]>[Si–H]) is obtained for N-rich silicon nitride. For silicon oxide (SiO_x), the same behavior is observed.[42] For low values of R, suboxide films ($x<2$) are obtained, with a significant concentration of Si–H bonds; while for high values of R stoichiometric SiO_2 films are obtained.

The same trend is observed for the $SiO_xN_yH_z$ films (see Fig. 4). For low values of R ($R<1$) Si-rich films are obtained, with higher concentrations of Si–H bonds than N–H bonds. As the parameter R is increased, the N–H bond concentration increases and the Si–H bond concentration decreases, becoming below detection limit for $R>3$.

These results can be explained by considering the mechanics of the deposition process. O–O, O–N, and N–N bonds are not stable and it can be assumed that these bonds are not present in the $SiO_xN_yH_z$ films.[32] Keeping in mind that each atom type comes from a single gas precursor (O atoms from O_2; N atoms from N_2; and Si atoms from SiH_4), the possible mechanisms for the film to grow are the following: reaction of O_2 and SiH_4 to form Si–O bonds; reaction of N_2 and SiH_4 to form Si–N and N–H bonds; and finally, reaction of SiH_4 with itself to form Si–Si and Si–H bonds. Here the term ''reaction'' is not quite exact, as the deposition process involves several intermediate steps; such as activation of the precursor gases, transport of the activated species to the substrate and surface reactions to grow the film.

All of the three above mentioned principal reaction chains are limited by the SiH_4 partial pressure, so that they are strongly competitive against each other. This result is evidenced by the behavior of the deposition rate shown in Fig. 4, which is much higher for the higher SiH_4 partial pressures during the deposition (lower values of R).

For high values of R (low SiH_4 partial pressure), the SiH_4 is almost totally consumed in the reactions with N_2 and O_2, so that the formation of Si–H bonds is negligible, as shown in Fig. 4. The formation of Si–Si bonds for these flow ratios is also expected to be very low. On the other hand, for low values of R there is excess of SiH_4 during the process that does not react with N_2 and O_2, and Si–H and Si–Si bonds are formed so that Si-rich films are obtained. These conclusions are similar to those reported by Smith for conventional PECVD processes.[43]

Concerning the formation of Si–O and Si–N bonds, as O_2 is much more reactive that N_2, the formation of Si–O bonds is predominant over the formation of Si–N bonds. For high values of the O_2 to SiH_4 ratio (parameter Q), almost all the SiH_4 reacts with O_2 and no significant amount of Si–N bonds is formed, so that oxide composition samples are obtained with $\alpha=1$, as shown in Fig. 1. Si–N bonds are only formed when the parameter Q is low enough to provide excess SiH_4 which can react with N_2. As the parameter Q is decreased, the formation of Si–N bonds is enhanced with respect to the formation of Si–O bonds and the composition approaches silicon nitride (i.e., α approaches zero).

For a given value of the parameter Q, a change in R may have a slight influence in the relative concentration of Si–O and Si–N bonds, as the N_2 to SiH_4 ratio would be affected. However, as shown in Fig. 1, it is the parameter Q which essentially determines the oxide fraction (parameter α) of the deposited films.

B. Structure of bonds

The structure of bonds of $SiO_xN_yH_z$ has been extensively discussed in the literature. Either the absorption coefficient or the imaginary part of the dielectric function may be studied for this analysis, as both magnitudes show characteristic bands of the specific molecular groups present in the material.

The most intense absorption signal in the $SiO_xN_yH_z$ system corresponds to the Si–O and Si–N stretching oscillations. For SiO_2 the Si–O stretching band has a characteristic wave number $\nu_{SiO}=1075\ cm^{-1}$,[44] while for Si_3N_4 the Si–N stretching band is located at $\nu_{SiN}=835\ cm^{-1}$.[21]

For $SiO_xN_yH_z$ films, many authors find a dominant absorption band, with a single maximum located at intermediate frequencies between those of SiO_2 and Si_3N_4.[1,11–13,30,45,46] This behavior is characteristic of single-phase homogeneous $SiO_xN_yH_z$ and its bonding structure is well described by the RBM previously explained [see Eq. (3)].

However, some authors find that the Si–O and Si–N stretching bands can be clearly distinguished in he absorption spectrum.[27,47] This is a strong indication that the RBM is not applicable and that the $SiO_xN_yH_z$ film is rather a mixture of two separate phases.

As shown in Fig. 7, the structure of bonds of our $SiO_xN_yH_z$ films is strongly dependent on the deposition parameter R. For $R<1$ the presence of two clearly distinct peaks (located at 872 and 1026 cm^{-1}) indicates that in these samples separation of two phases occur. However, as these peaks are slightly shifted with respect to the characteristic frequencies of the Si–N and Si–O stretching oscillations in

Si_3N_4 and SiO_2 ($\nu_{SiN}=835\ cm^{-1}$ and $\nu_{SiO}=1075\ cm^{-1}$, respectively), it is suggested that some tetrahedrons of the type SiO_jN_{4-j} involving both N and O atoms may also be present. The behavior of the Si–H stretching band, with two distinct peaks for $R<1$ (Fig. 5), is consistent with the conclusions derived from the Si–O/Si–N band.

It is suggested that the separation of two phases observed in these films is related to the comparatively high relative Si content corresponding to the low values of R during deposition. This proposal is consistent with the results of Cros *et al.*,[27] who found similar spectra in Si-rich films.

As the parameter R is increased, the separation of two phases becomes less clear. For $R=1.3$ still two bands can be distinguished, but the Si–O peak appears at lower wave numbers ($1011\ cm^{-1}$) and the Si–N peak looks like a shoulder in the band rather than like an independent peak. In these samples there is still a significant separation of phases, but the amount of intermediate SiO_jN_{4-j} tetrahedrons ($j=1,2,3$) is higher.

For $R=1.6$ there is a single maximum located at $972\ cm^{-1}$ which can no longer be attributed just to the Si–O vibration, but rather to the combined contribution of different SiO_jN_{4-j} tetrahedrons. Still, a shoulder in the band at the wave number corresponding to the Si–N vibration is outlined, suggesting a certain degree of separation of two phases. This conclusion is supported by the EPR spectra shown in Fig. 11, in which two different signals, one characteristic of SiN_yH_z (K center), and the other characteristic of SiO_2 (E' center) are observed. For this value of R, a single peak which shifts to higher wave numbers as the composition parameter α increases was appreciated in the Si–H stretching band (Fig. 6). It must be taken into account that the EPR technique is much more sensitive than FTIR spectroscopy. Furthermore, the Si–H concentration for samples of series R1.6 is relatively low, so that the Si–H stretching band is weak and it is difficult to resolve its fine structure. It is concluded that for $R=1.6$ near single-phase films are obtained, with a certain degree of separation of two phases.

For higher values of R ($R>3$), the trend goes on, with the shoulder becoming less clear so that the samples basically can be regarded as single phase. This conclusion is supported by the behavior of the band shown in Fig. 8 for the samples deposited at $R=5.0$: a continuous shift from the characteristic wave number of SiN_yH_z to that of SiO_2, as composition is changed. Also, the EPR spectra for $R=5.0$ shows a single feature.

Additionally, for the single-phase samples, the maximum value of the FWHM of the Si–O/Si–N band was obtained for the exact middle composition $\alpha=0.5$ (Fig. 9). This is precisely the composition for which the maximum dispersion of different chemical environments is predicted by the RBM (Fig. 10). So, the results obtained are well in accordance with the RBM.

V. CONCLUSIONS

$SiO_xN_yH_z$ films were deposited at room temperature from O_2, N_2, and SiH_4 gas mixtures. The correlation between the optical and structural properties, the composition and the deposition parameters was studied. A sensitive and comparatively accurate measurement of the absolute concentration of all involved film components (including hydrogen) was performed by HI-ERDA. By an adequate control of the precursor gas flow ratios, samples with compositions covering the whole range between silicon nitride and silicon oxide were obtained. The incorporation of H in the films results in lower concentrations of Si and N than in stoichiometric films, especially for compositions close to silicon nitride, in which the H content is higher.

As O_2 is much more reactive than N_2, the relative incorporation of O and N in the films is essentially determined by the parameter $Q=\phi(O_2)/\phi(SiH_4)$, while the SiH_4 partial pressure during deposition, $R=[\phi(O_2)+\phi(N_2)]/\phi(SiH_4)$, determines the relative content of Si in the films.

For samples deposited at high SiH_4 partial pressures (low values of R), evidence of separation of two phases is observed, as the Si–N and Si–O stretching bands can be clearly distinguished. Additionally, the Si–H stretching band shows separate peaks for the $(N_3)-SiH/(SiN_2)-Si-H$ and the $(O_3)-Si-H/(SiO_2)-SiH$ configurations. Also, the signals due to the K and E' centers are separated in the EPR spectrum.

On the other hand, for samples deposited at low SiH_4 partial pressures, a single Si–O/Si–N stretching band that shifts from the wave number of silicon nitride to the value of silicon oxide as the composition changes is observed. Similar results are observed for the Si–H band. This behavior, together with a maximum value of the FWHM of the Si–O/Si–N stretching band for middle compositions is characteristic of single-phase homogeneous samples, with a structure of bonds in agreement with the RBM.

It was possible to control the refractive index value over the whole range between silicon nitride and silicon oxide. The obtained values are slightly lower than in stoichiometric films as the incorporation of H results in a lower film density.

The most important defect types observed in the EPR spectrum were the Si dangling bonds: the K center and the E' center, with some variants. Defects directly related to the presence of N were also observed. The overall defect density was highest for silicon nitride films and remained roughly constant over the whole composition range of $SiO_xN_yH_z$ films. For SiO_2 the density of defects is significantly lower than in the $SiO_xN_yH_z$ films.

All these findings show that the ECR–PECVD technique is well studied to produce $SiO_xN_yH_z$ films at room temperature, with specific and reproducible properties to be fitted to different applications in the microelectronics industry.

ACKNOWLEDGMENTS

The authors acknowledge C. A. I. de Impalntación Iónica (U. C. M.) for availability of deposition system and Dr. E. Iborra (E. T. S. I. T. Universidad Politécnica de Madrid) for availability of FTIR spectrometer. The work has been partially financed by the CICYT (Spain) under Contract No. TIC 01-1253. Technical support of G. Keiler is gratefully acknowledged.

[1] Y. Ma and G. Lucovsky, J. Vac. Sci. Technol. B **12**, 2504 (1994).
[2] L. Manchanda, G. R. Weber, Y. O. Kim, L. C. Feldman, N. Moryia, B. E. Weir, R. C. Kistler, M. L. Green, and D. Brasen, Microelectron. Eng. **22**, 69 (1993).
[3] E. C. Carr and R. A. Buhrman, Appl. Phys. Lett. **63**, 54 (1993).
[4] T. Arakawa, R. Matsumoto, and A. Kita, Jpn. J. Appl. Phys., Part 1 **35**, 1491 (1996).
[5] W. A. P. Claassen, H. A. J. Th. v. d. Pol, A. H. Goemans, and A. E. T. Kuiper, J. Electrochem. Soc. **133**, 1458 (1986).
[6] P. V. Bulkin, P. L. Swart, and B. M. Lacquet, J. Non-Cryst. Solids **187**, 484 (1995).
[7] S. Callard, A. Gagnaire, and J. Joseph, J. Vac. Sci. Technol. A **15**, 2088 (1997).
[8] F. Gaillard, P. Schiavone, and P. Brault, J. Vac. Sci. Technol. A **15**, 2777 (1997).
[9] H. T. Tang, W.N. Lennard, C. S. Zhang, K. Griffiths, B. Li, L. C. Feldman, and M. L. Green, J. Appl. Phys. **80**, 1816 (1996).
[10] I. J. R. Baumvol, F. C. Stedile, J.-J. Ganem, I. Trimaille, and S. Rigo, Appl. Phys. Lett. **70**, 2007 (1997).
[11] L.-N. He, T. Inokuma, and S. Hasegawa, Jpn. J. Appl. Phys., Part 1 **35**, 1503 (1996).
[12] S. V. Hattangady, H. Niimi, and G. Lucovsky, J. Vac. Sci. Technol. A **14**, 3017 (1996).
[13] M. J. Hernández, J. Garrido, J. Martínez, and J. Piqueras, Semicond. Sci. Technol. **12**, 927 (1997).
[14] A. del Prado, I. Mártil, M. Fernández, and G. González-Díz, Thin Solid Films **343–344**, 432 (1999).
[15] A. del Prado, F. L. Martínez, M. Fernández, I. Mártil, and G. González-Diaz, J. Vac. Sci. Technol. A **17**, 1263 (1999).
[16] S. Garcia, J. M. Martin, M. Fernández, I. Mártil, and G. González-Diaz, Philos. Mag. **73**, 487 (1996).
[17] F. L. Martinez, I. Mártil, G. González-Diaz, B. Selle, and I. Sieber, J. Non-Cryst. Solids **227–230**, 523 (1998).
[18] W. Bohne, J. Röhrich, and G. Röschert, Nucl. Instrum. Methods Phys. Res. B **136–138**, 633 (1998).
[19] W. Bohne, W. Fuhs, J. Röhrich, B. Selle, I. Sieber, A. del Prado, E. San Andrés, I. Mártil, and G. González-Diaz, Surf. Interface Anal. **34**, 749 (2002).
[20] W. A. Lanford and M. J. Rand, J. Appl. Phys. **49**, 2473 (1978).
[21] T. S. Eriksson and C. G. Granqvist, J. Appl. Phys. **60**, 2081 (1986).
[22] A. del Prado, E. San Andrés, F. L. Martínez, I. Mártil, G. González-Diaz, W. Bohne, J. Röhrich, B. Selle, and M. Fernández, Vacuum **67**, 507 (2002).
[23] S. M. Sze, *Physics of Semiconductor Devices* (Wiley, New York, 1981).
[24] A. Sassella, P. Lucarno, A. Borghesi, F. Corni, S. Rojas, and L. Zanotti, J. Non-Cryst. Solids **187**, 395 (1995).
[25] G. Lucovsky, Solid State Commun. **29**, 571 (1979).
[26] J.-L. Yeh and S.-C. Lee, J. Appl. Phys. **79**, 656 (1996).
[27] Y. Cros and J. C. Rostaing, Proceedings E: Materials Research Society, Strasbourg, June 1986, p. 77.
[28] G. Lucovsky, J. Yang, S. S. Chao, J. E. Tyler, and W. Czubatyj, Phys. Rev. B **28**, 3234 (1983).
[29] A. Sassella, A. Borghesi, F. Corni, A. Monelli, G. Ottaviani, R. Tonini, B. Pivac, M. Bacchetta, and L. Zanotti, J. Vac. Sci. Technol. A **15**, 377 (1997).
[30] D. V. Tsu, G. Lucovsky, M. J. Mantini, and S. S. Chao, J. Vac. Sci. Technol. A **5**, 1998 (1987).
[31] H. R. Philipp, J. Non-Cryst. Solids **8–10**, 627 (1972).
[32] A. Sassella, Phys. Rev. B **48**, 14208 (1993).
[33] J. S. Blakemore, *Solid State Physics* (Cambridge University Press, Cambridge, 1985).
[34] W. L. Warren, J. Kanicki, F. C. Rong, and E. H. Poindexter, J. Electrochem. Soc. **139**, 880 (1992).
[35] W. L. Warren, E. H. Poindexter, M. Offenberg, and W. Müller-Warmuth, J. Electrochem. Soc. **139**, 872 (1992).
[36] W. L. Warren, P. M. Lenahan, and S. E. Curry, Phys. Rev. Lett. **65**, 207 (1990).
[37] S. Hasegawa, S. Sakamori, M. Futatsudera, T. Inokuma, and Y. Kurata, J. Appl. Phys. **89**, 2598 (2001).
[38] J. H. Stathis, J. Chapple-Sokol, E. Tierney, and J. Batey, Appl. Phys. Lett. **56**, 2111 (1990).
[39] T. E. Tsai, D. L. Griscom, and E. J. Friebele, Phys. Rev. B **38**, 2140 (1988).
[40] E. San Andrés, A. del Prado, I. Mártil, G. González-Diaz, F. L. Martinez, D. Bravo, F. J. López, and M. Fernández, Vacuum **67**, 525 (2002).
[41] F. L. Martínez, A. del Prado, I. Mártil, G. González-Diaz, W. Bohne, W. Fuhs, J. Röhrich, and B. Selle, Phys. Rev. B **63**, 245320 (2001).
[42] E. San Andrés, A. del Prado, I. Mártil, G. González-Diaz, D. Bravo, and F.J. López, J. Appl. Phys. **92**, 1906 (2002).
[43] D. L. Smith, J. Vac. Sci. Technol. A **11**, 1843 (1993).
[44] P. G. Pai, S. S. Chao, Y. Takagi, and G. Lucovsky, J. Vac. Sci. Technol. A **4**, 689 (1986).
[45] C. M. M. Denisse, K. Z. Troost, J. B. Oude Elferink, F. H. P. M. Habraken, W. F. van der Weg, and M. Hendriks, J. Appl. Phys. **60**, 2536 (1986).
[46] B.-R. Zhang, Z. Yu, G. J. Collins, T. Hwang, and W. H. Ritchie, J. Vac. Sci. Technol. A **7**, 176 (1989).
[47] L. Pinard and J. M. Mackowski, Appl. Opt. **36**, 5451 (1997).